BAMS Supplement

New Era of Air Quality Monitoring from Space

Geostationary Environment Monitoring Spectrometer (GEMS)

Jhoon Kim, Ukkyo Jeong, Myoung-Hwan Ahn, Jae H. Kim, Rokjin J. Park, Hanlim Lee, Chul Han Song, Yong-Sang Choi, Kwon-Ho Lee, Jung-Moon Yoo, Myeong-Jae Jeong, Seon Ki Park, Kwang-Mog Lee, Chang-Keun Song, Sang-Woo Kim, Young Joon Kim, Si-Wan Kim, Mijin Kim, Sujung Go, Xiong Liu, Kelly Chance, Christopher Chan Miller, Jay Al-Saadi, Ben Veihelmann, Pawan K. Bhartia, Omar Torres, Gonzalo González Abad, David P. Haffner, Dai Ho Ko, Seung Hoon Lee, Jung-Hun Woo, Heesung Chong, Sang Seo Park, Dennis Nicks, Won Jun Choi, Kyung-Jung Moon, Ara Cho, Jongmin Yoon, Sang-kyun Kim, Hyunkee Hong, Kyunghwa Lee, Hana Lee, Seoyoung Lee, Myungje Choi, Pepijn Veefkind, Pieternel F. Levelt, David P. Edwards, Mina Kang, Mijin Eo, Juseon Bak, Kanghyun Baek, Hyeong-Ahn Kwon, Jiwon Yang, Junsung Park, Kyung Man Han, Bo-Ram Kim, Hee-Woo Shin, Haklim Choi, Ebony Lee, Jihyo Chong, Yesol Cha, Ja-Ho Koo, Hitoshi Irie, Sachiko Hayashida, Yasko Kasai, Yugo Kanaya, Cheng Liu, Jintai Lin, James H. Crawford, Gregory R. Carmichael, Michael J. Newchurch, Barry L. Lefer, Jay R. Herman, Robert J. Swap, Alexis K. H. Lau, Thomas P. Kurosu, Glen Jaross, Berit Ahlers, Marcel Dobber, C. Thomas McElroy, and Yunsoo Choi

https://doi.org/10.1175/BAMS-D-18-0013.2
Corresponding author: Jhoon Kim, jkim2@yonsei.ac.kr
This document is a supplement to https://doi.org/10.1175/BAMS-D-18-0013.1

The information presented here is supplemental to the main paper. The section "User requirements" is a collection of figures and tables related to the development of user requirements for Geostationary Environment Monitoring Spectrometer (GEMS). The section "Preflight tests" is a complimentary descriptions of instrument characterization before integration to spacecraft. The section "L1 and L2 processors" includes detail flowchart of level-1 (L1) and level-2 (L2) processors with descriptions. The section "Expected performance" is a collection of figures and a table related to the predicted performance of GEMS using optimal estimation. The section "Retrieval sensitivity for ozone" is a collection of averaging kernels in January to show its diurnal variations. The section "Validation network" is a summary of available observations from the ground-based network within the GEMS domain. Finally, the section "Geostationary AQ constellation" includes a detailed description of NASA's Tropospheric Emissions: Monitoring of Pollution (TEMPO) and ESA's Sentinel-4 Mission.

Table ES1. Major user requirements of GEMS.

System attributes	Requirements
Lifetime	>10 years
Reliability	>0.85 at EOL
Field of regard	>5,000 km (N/S) × 5,000 km (E/W) N/S range: 45°N–5°S E/W range: Selectable between 75° and 145°E Orbital position:116.2°E < position < 128.2°E
Duty cycle/imaging time	Eight images during daytime (30 min imaging + 30 min rest) × 8 times day^{-1}
Ground sampling distance	<7 km (N/S) at Seoul GSD area < 56 km^2 at Seoul (aspect ratio less than 1:3)
Spectral range	300 to 500 nm
Spectral resolution	<0.6 nm
Spectral sampling	<0.2 nm
Signal-to-noise ratio	>720 at 320 nm >1,500 at 430 nm
Data quantization	≥12 bits
MTF (instrument level)	>0.3 in N/S direction at Nyquist frequency >0.3 in E/W direction at Nyquist frequency
Imaging navigation	1 pixel
Pointing stability	48 μrad 2 s^{-1}
Pointing accuracy	0.02°
Radiometric calibration accuracy	<4% (including standard lamp uncertainty)
Spectral calibration accuracy	<0.02 nm
Spectral calibration stability	<0.02 nm (within daytime observations)
Polarization factor	<2% (310–500 nm) No inflection point within any 20 nm range
Spectral feature	<0.05% (within 3 nm)
Stray light	<2% (310–500 nm)

User requirements

Table ES1 lists major user requirements including spatial and temporal resolution, spectral sampling, and SNR. Figures ES1–ES3 show analyses of the spatial, radiometric, and spectral requirements. The spatial coverage of GEMS was selected to cover important emission source regions in Asia (Fig. 5). After analyzing long-term MODIS cloud products, the spatial resolution was selected to be 7 km × 8 km at Seoul to optimize the probability of finding clear-sky pixels and retain the capability to cover a wide field of regard (FOR) within 30 min. Spatial resolution, FOR, and data rate are optimized for the GEMS observation strategy. Increasing from a spatial resolution of 7 km × 8 km, the probability of finding clear-sky pixels does not improve significantly until reaching 2 km × 2 km (Fig. ES1). Radiance spectra are provided by binning two 3.5 km × 8 km pixels, to meet the SNR requirements. As shown in the Fig. ES1, the probability of finding clear-sky pixels drops by 15% to 30% for 15 km × 15 km resolution, compared with 7 km × 8 km. Additional cloud information can be obtained with high spatial resolution from Advanced Meteorological Imager (AMI) on board *Geostationary Korea Multi-Purpose Satellite 2A* (*GK-2A*) with full disk coverage every 10 min.

The spectral range was chosen to cover the absorption lines of the gases of interest (Fig. 3). For aerosol property retrievals, measurements in the longer visible (Vis) and near-infrared (NIR) regions are useful, but a measurement window in the UV–Vis region, similar to that of Ozone Monitoring Instrument (OMI), was eventually chosen for GEMS. The spectral resolution was selected to be 0.6 nm with 3 samples/band, based on sensitivity tests using resampled OMI spectra and simulations using radiative transfer models (RTMs). The accuracy of the O_3, SO_2, and HCHO retrievals is sensitive to the spectral resolution (Fig. ES2), and contributed to

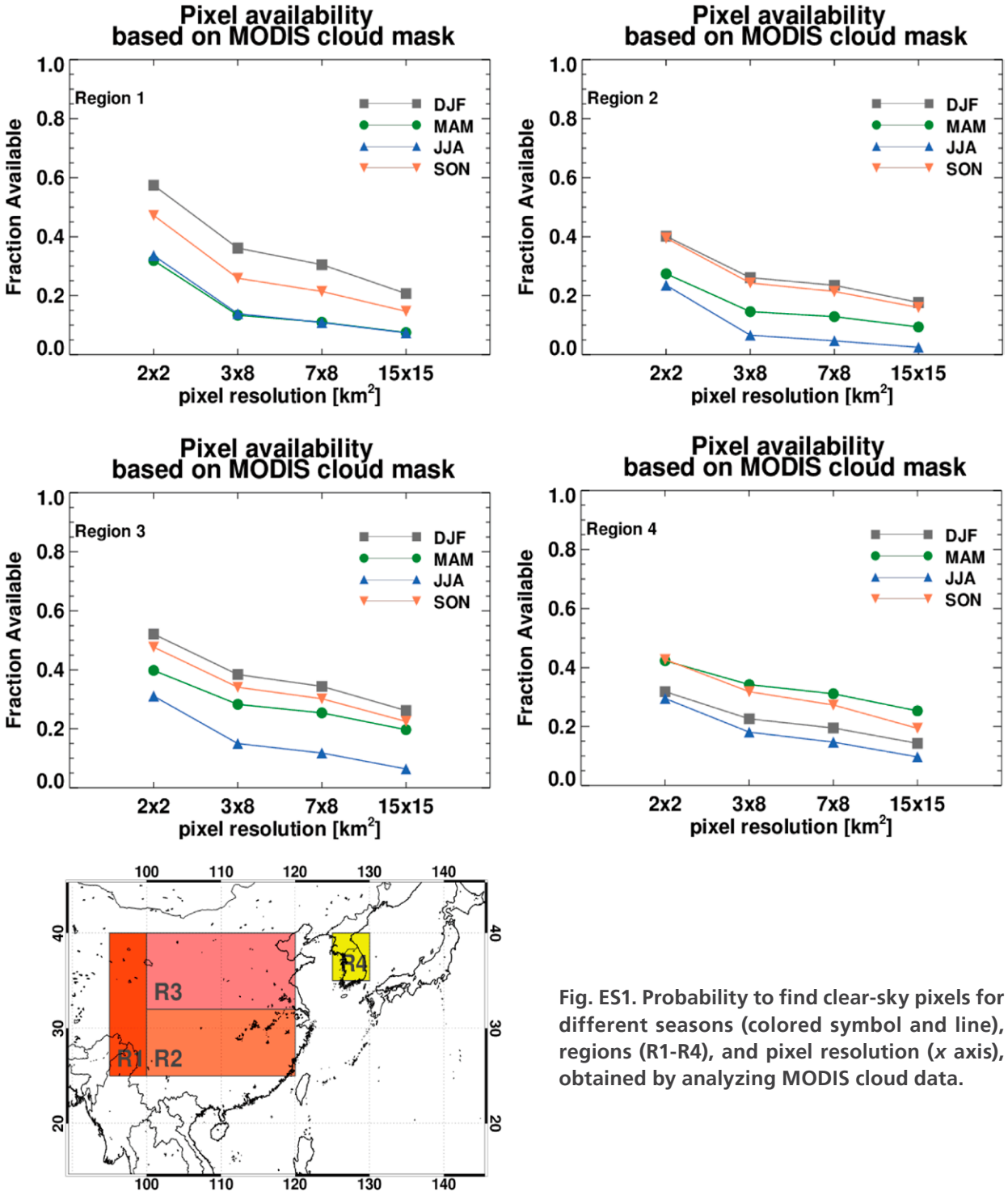

Fig. ES1. Probability to find clear-sky pixels for different seasons (colored symbol and line), regions (R1-R4), and pixel resolution (*x* axis), obtained by analyzing MODIS cloud data.

the user requirements. Because the spectral resolution affects the SNR, the spectral resolution was optimized to produce product uncertainties small enough to resolve air quality (AQ) standards and achieve the required accuracy (Fig. ES3). The 1σ uncertainties for the various gas products can be reduced by increasing SNRs, which can be achieved by binning multiple spatial pixels.

Figure ES4 shows solar illumination conditions for different seasons as solar zenith angle (SZA) contours by season. Using these SZAs, an ideal E–W scan scenario was suggested (Fig. ES5). GEMS scans from east to west and return to null position to be ready for next scan. However, due to the limited number of command lines on board the GK-2B spacecraft, this was optimized to the 3-scan scenario shown in Fig. 5.

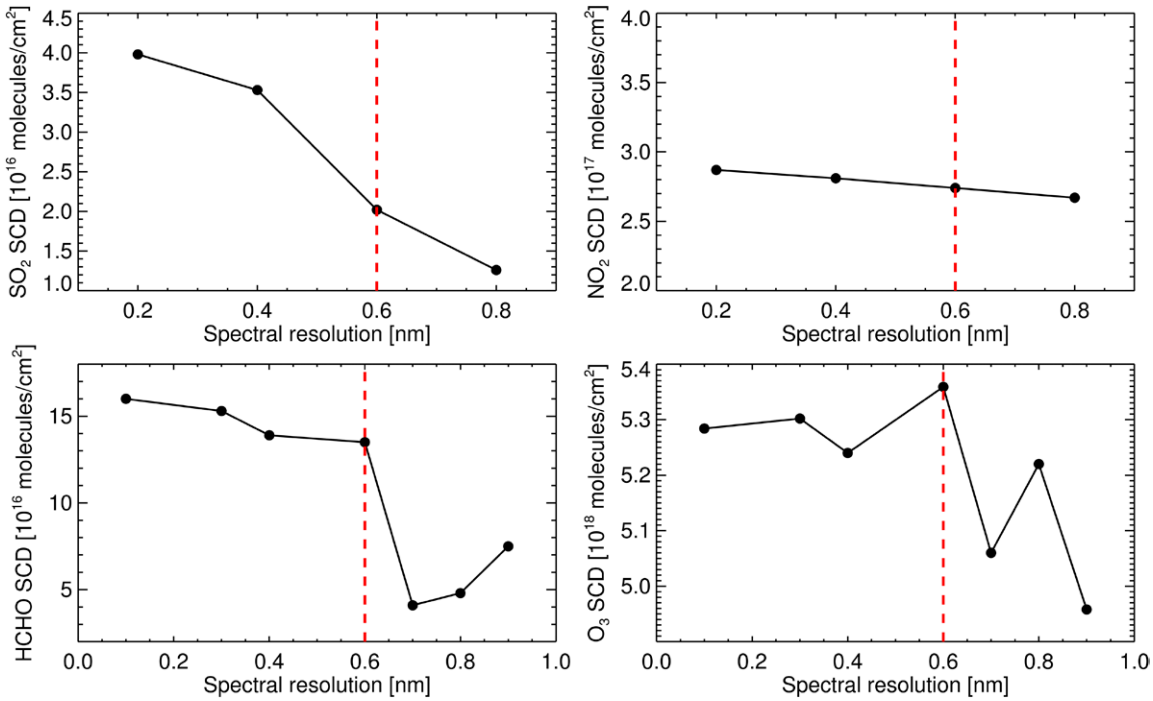

Fig. ES2. Retrieved slant column densities (SCDs) for different gases (*y* axis) as a function of spectral resolution (*x* axis), by resampling high-resolution simulated radiance spectra. True SCD values are assumed for the highest spectral resolution calculated by the radiative transfer model, and DOAS retrieved values are shown in the *y* axes.

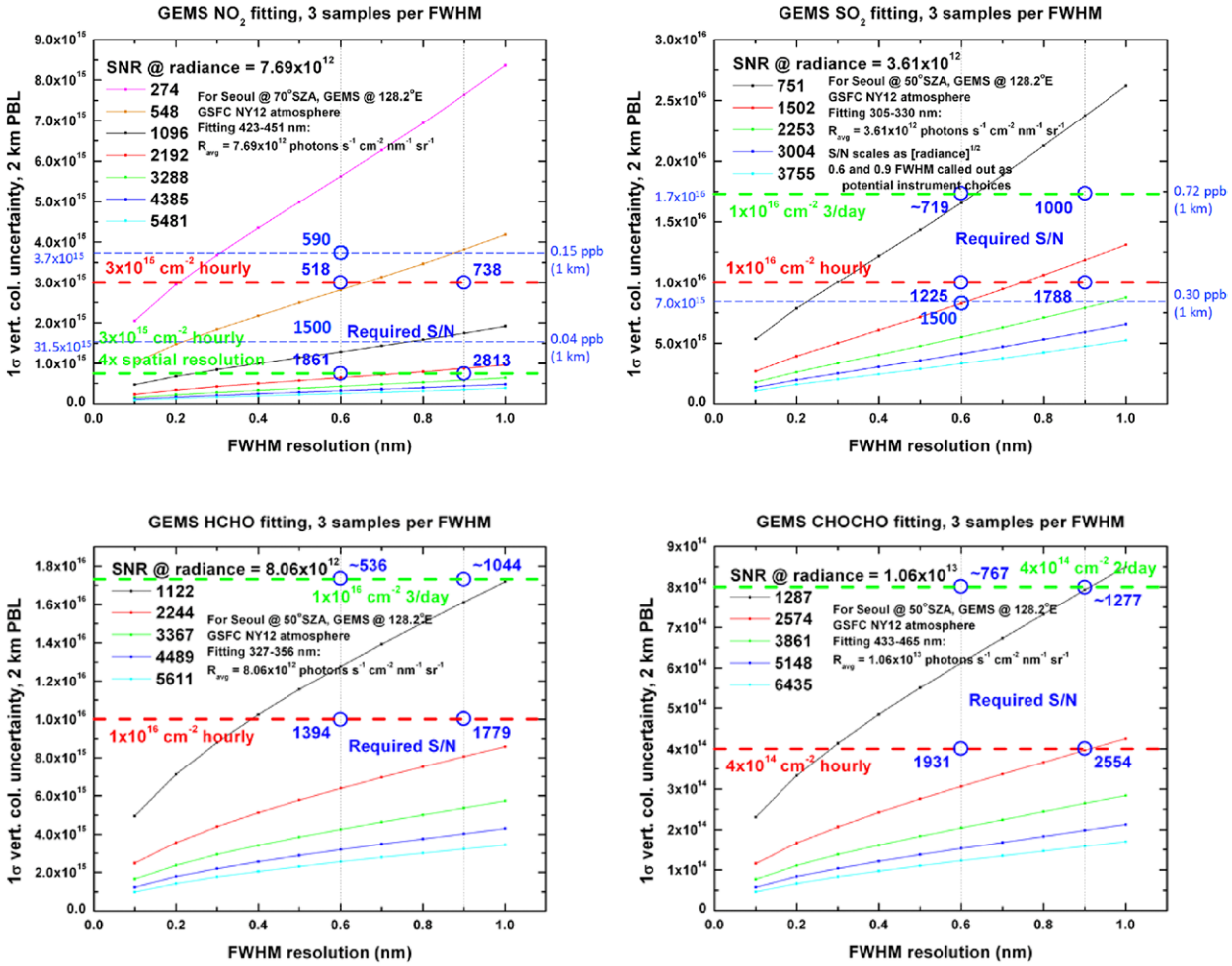

Fig. ES3. Analysis of SNR for NO_2, SO_2, HCHO, and CHOCHO for FWHM resolution (abscissas) and 1σ uncertainty in vertical column density (ordinates). Different colors represent different SNRs as indicated in legend. Following the dotted vertical line at a given FWHM of 0.6 nm, 1σ uncertainty can be estimated for corresponding SNR values.

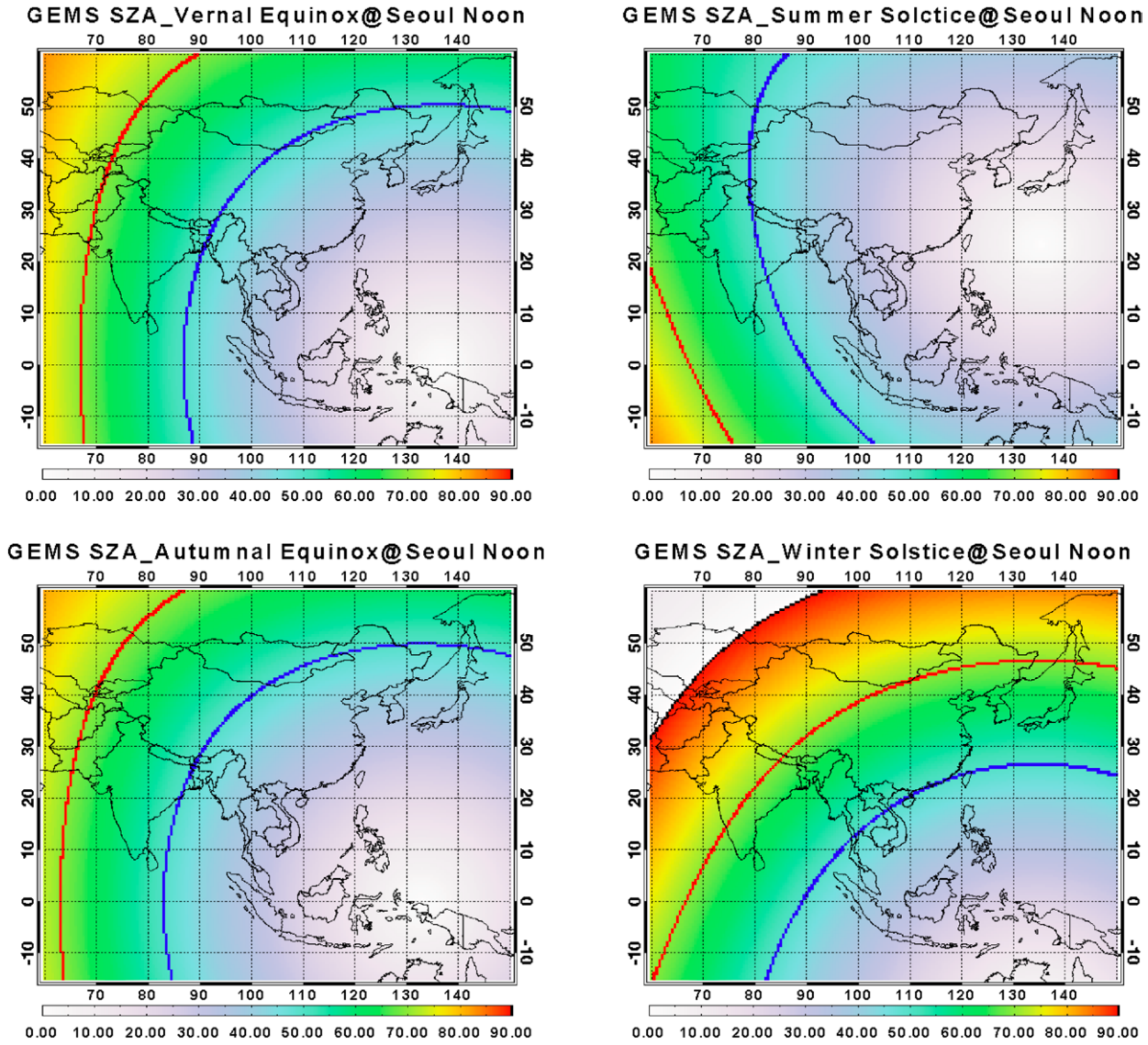

Fig. ES4. Solar zenith angles (SZA) distributions for different seasons within the GEMS FOR. Blue, red, and black lines represent SZA of 50, 70, and 90, respectively.

Preflight tests

Prior to the final assembly of the GEMS with the spacecraft, GEMS went through characterization and calibration tests to confirm compliances with the GEMS requirements and to gather GEMS sensor data that are critical for on-ground corrections. The spatial, spectral, and radiometric performances of the GEMS were tested.

For the spatial performance test, a tunable laser feeds a pinhole target placed at the focus of the GEMS instrument system. GEMS spectral performances are verified at the spectrometer level only, using *f*-number matched broadband or monochromatic light in front of the slit in the spectrometer. As radiometric calibration and polarization tests need high SNR during the test, radiometric performance is characterized using the thermal vacuum test configuration. Major user requirements of the GEMS instrument are listed in Table ES1.

L1 and L2 processor

A flowchart of processing from L0 to L2 is shown in Fig. ES6. Level 1B data are spectrally, radiometrically, and geometrically calibrated from the transmitted L0 digital count value. The baseline L1b processor consists of sequences of image corrections followed by spectral registration and radiometric calibrations. The processor applies to both Earth radiance and solar irradiance calibration in which the diffuser bidirectional transmittance distribution

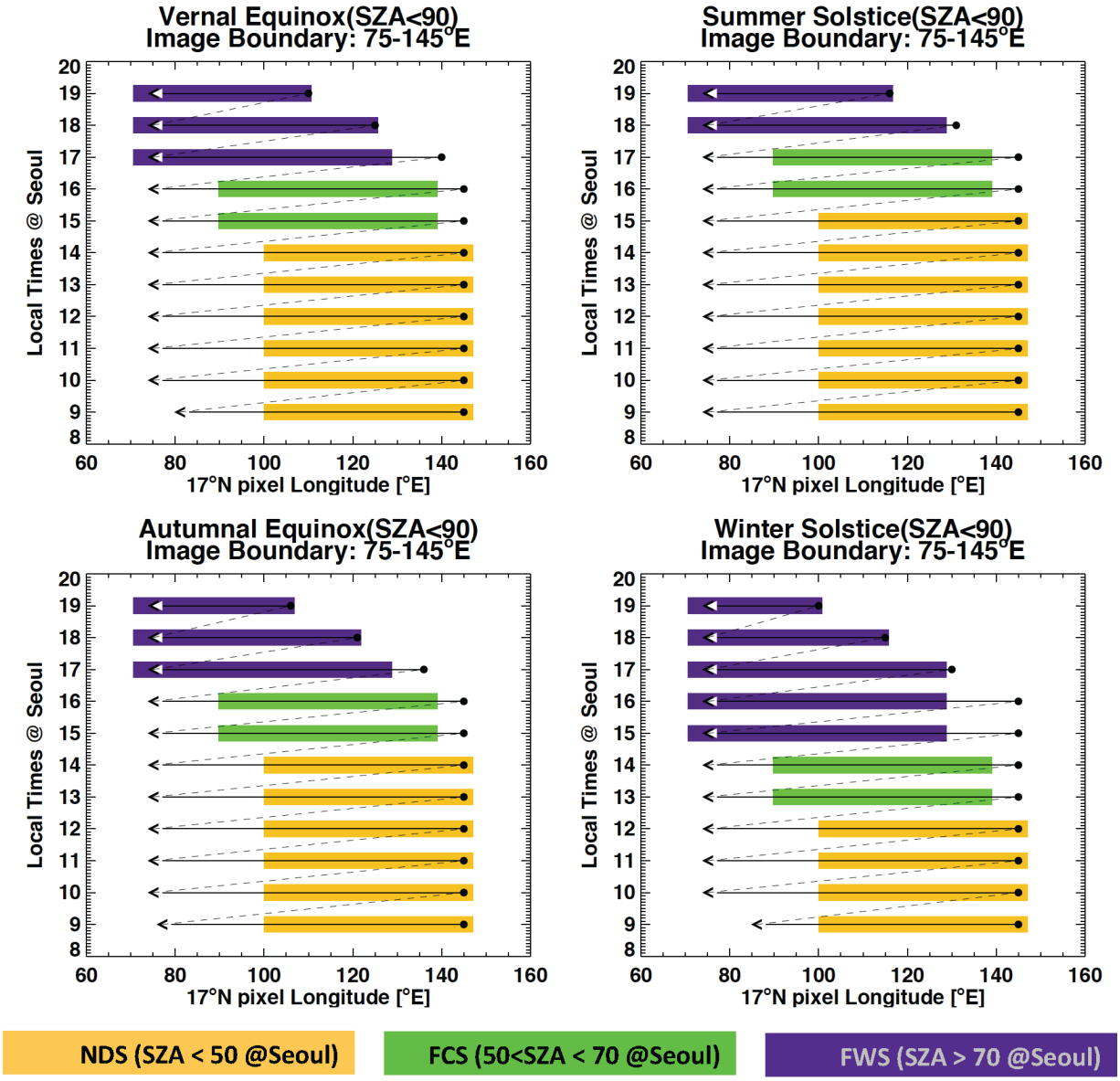

Fig. ES5. Ideal E–W scan scenarios (black solid lines) for different seasons. Vertical and horizontal axes represent local time in Seoul and pixel longitude at 17°N. Dashed lines represent scan mirror movement back to null position after scan. Nominal daily scan (NDS), full central scan (FCS), and full west scan (FWS) represent scan scenarios of GEMS in Fig. 5.

function (BTDF) correction is applied. After these steps, spatial registration, and spectral and radiometric calibration are done for the Earth radiance, and spatial registration and BTDF/goniometry calibrations are performed for the solar irradiance.

The L2 processor uses L1b data to provide the final scientific products, as described in section 3. As the polarization correction is dependent on geometry of observation, it is done after the image navigation and registration (INR). All GEMS data are received and processed at the Environmental Satellite Center (ESC) of the National Institute of Environmental Research (NIER). All data are processed from L0 to L3 at ESC where the final data will be distributed to users via the Internet. Further details can be found in W. J. Choi et al. (2018).

Expected performance

The expected retrieval performance of GEMS was assessed according to its design requirements, prelaunch calibration results, and synthetic radiances using the optimal estimation (OE) method (Rodgers 2000; Jeong 2015). This method classifies sources of the retrieval error into five categories (i.e., smoothing error, model parameter error, forward model error, systematic

measurement error, and retrieval precision; Rodgers 2000). The calculated retrieval errors for trace gases include both systematic and random components from measurement uncertainties, interferences from spectral absorptions by other species, spectroscopic parameter errors, surface reflectance uncertainty, and other ancillary information uncertainties. Errors in radiances and irradiances are precisely estimated at high precision from prelaunch calibration, including radiometric calibration, polarization sensitivity, and stray light. The vector linearized discrete ordinate radiative transfer code (VLIDORT) model was used to generate GEMS synthetic radiances from hourly simulated trace gases and aerosol concentrations from a GEOS-5 nature run (Molod et al. 2015), and surface reflectance from OMI climatology (Kleipool et al. 2008).

To retrieve trace gas concentrations, the absorption signal of the target species must be sufficiently large compared with the measurement noise. Physical parameters such as the vertical profiles of trace gases and surface reflectance also affect the measurement sensitivity. Longer optical pathlength through the layers of trace gases, as well as the sufficient numbers of photons reaching at the detector, provide better measurement sensitivity. Estimated retrieval errors of the GEMS trace gases as a function of SZA are shown in Fig. ES7 and Table ES2. The retrieval errors increase with SZA for all gases except for NO_2. GEMS is expected to provide reliable diurnal cycles of NO_2 at all SZAs, as the fitting window is at longer wavelengths than that of other gases (Table 2), and is thus less shielded by Rayleigh scattering even at higher SZAs (Fig. ES7a). The expected retrieval accuracy of HCHO from GEMS also satisfies the user requirements up to a SZA of ~70° (Fig. ES7c), whereas that of SO_2 decreases significantly at SZA > 50° (Fig. ES7b). The tropospheric ozone retrievals from GEMS might have higher retrieval errors at larger SZA > 70°. However, stratospheric ozone is of uniform quality for the full diurnal cycle. In addition to the viewing geometry, persistent aerosols over East Asia along with diverse surface types,

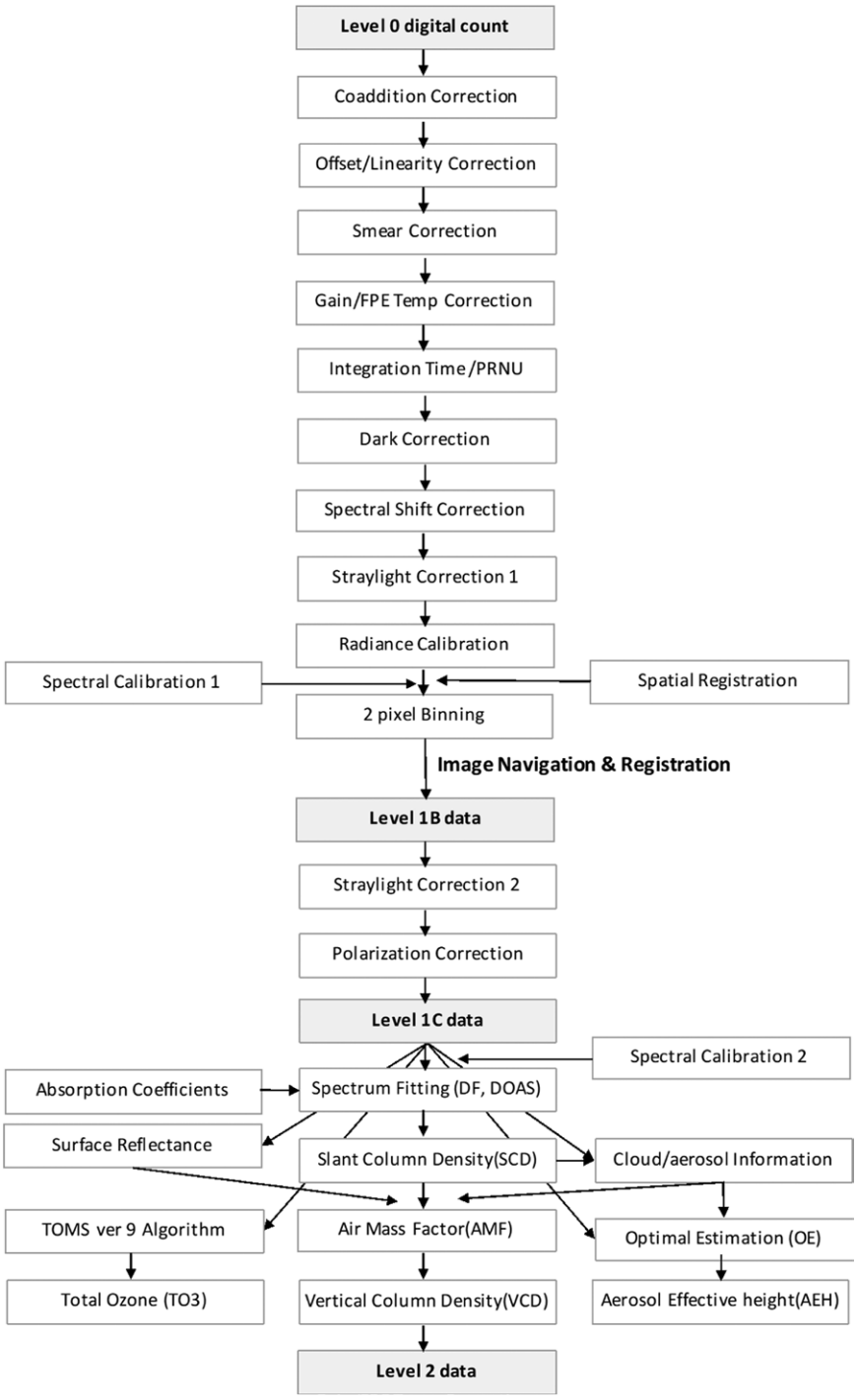

Fig. ES6. Flowchart of the GEMS level-1 and level-2 processors.

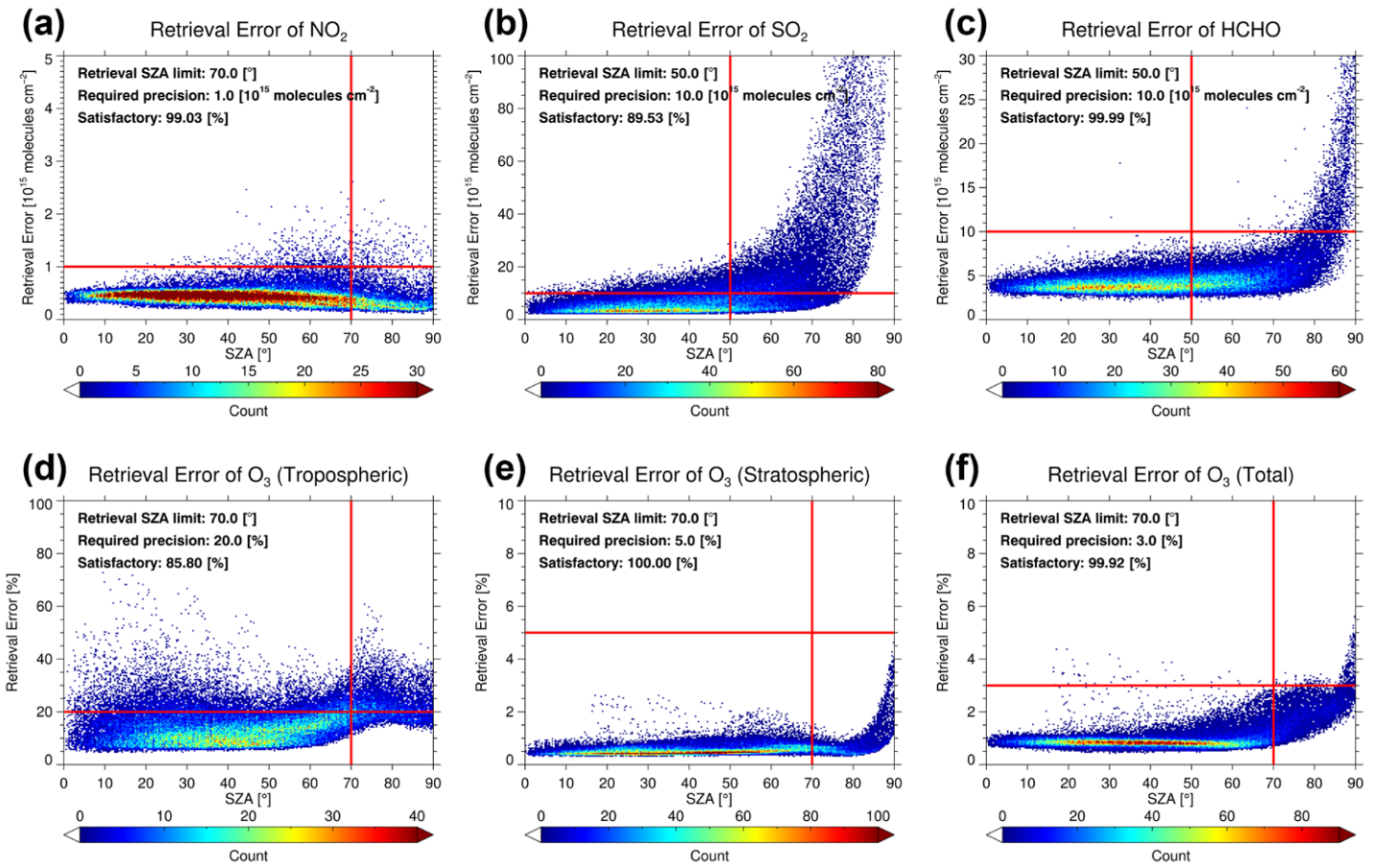

Fig. ES7. The estimated retrieval errors of (a) NO_2, (b) SO_2, (c) HCHO, (d) tropospheric O_3, (e) stratospheric O_3, and (f) total O_3 VCD as functions of SZA. Vertical and horizontal red lines represent user requirements in uncertainty and SZA, respectively; thus, data points below and to the left of these red lines satisfy requirements.

Table ES2. Statistics and requirement satisfaction of estimated retrieval error of GEMS target trace gases.

Target product (unit)	Retrieval error				Requirement satisfaction
	Mean ± std dev	Median	Maximum	Minimum	
NO_2 (10^{15} molecules cm^{-2})	0.45 ± 0.13	0.44	2.47	0.15	99.03%
SO_2 (10^{15} molecules cm^{-2})	5.81 ± 3.07	4.87	28.90	2.06	89.53%
HCHO (10^{15} molecules cm^{-2})	4.03 ± 0.81	3.86	17.77	2.02	99.99%
Tropospheric O_3 (%)	3.33 ± 1.29	2.93	18.49	1.64	85.80%
Stratospheric O_3 (%)	1.43 ± 0.59	1.23	6.38	0.76	100.00%
Total O_3 (%)	2.54 ± 0.80	2.33	12.37	1.43	99.92%

Table ES3. Classified sources of retrieval error for each retrieval target species of GEMS.

Target product (unit)	Error sources of retrieval error			
	Solution error	Albedo uncertainty	Polarization residual	Stray light residual
NO_2 (10^{15} molecules cm^{-2})	0.44 ± 0.11	0.02 ± 0.09	0.06 ± 0.05	0.00 ± 0.00
SO_2 (10^{15} molecules cm^{-2})	5.79 ± 3.04	0.23 ± 0.50	0.05 ± 0.07	0.14 ± 0.13
HCHO (10^{15} molecules cm^{-2})	3.74 ± 0.62	0.16 ± 0.16	1.08 ± 1.11	0.20 ± 0.04
Tropospheric O_3 (%)	2.24 ± 0.86	1.38 ± 1.48	0.06 ± 0.06	1.45 ± 0.93
Stratospheric O_3 (%)	1.26 ± 0.52	0.39 ± 0.37	0.03 ± 0.03	0.38 ± 0.33
Total O_3 (%)	1.47 ± 0.43	1.29 ± 1.05	0.04 ± 0.04	1.24 ± 0.68

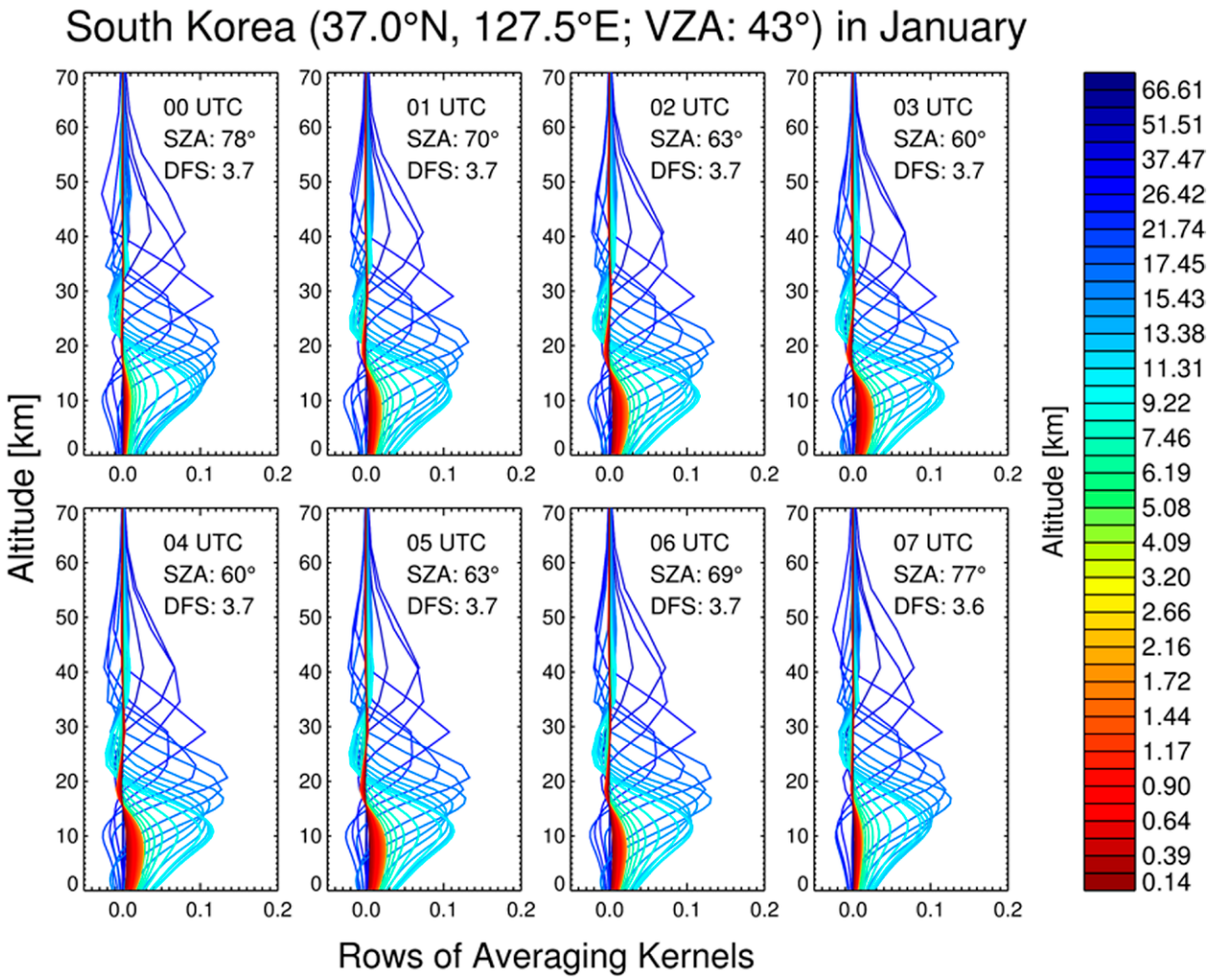

Fig. ES8. Rows of the averaging kernel matrices of O_3 profile retrievals throughout the day (0000–0700 UTC) for 15 Jan in Seoul. The values were normalized by the variability of the O_3 at each altitude (from Jeong 2015). Colors represent values at different peak altitudes.

contribute to overall trace gas errors. Table ES3 shows the classified sources of retrieval error for each retrieval target species of GEMS.

The effect of aerosols and surface reflectance on trace gas retrieval is also important, particularly in East Asia. Absorbing aerosols typically reduces the light pathlength, thus reducing measurement sensitivity. The role of scattering aerosols is more complicated as it depends on the relative vertical distributions. Scattering aerosols above the target trace gases lead to reduced gaseous absorption, and consequently, reduced signal and retrieval sensitivity. The opposite is true for scattering aerosols below the target gases (Jeong 2015). However, the effects of aerosols and surface reflectance on trace gas retrievals can be minimized by their careful characterization.

Retrieval sensitivity for ozone

Ozone is a key component of GEMS retrievals, as it affects the accuracy of other trace gas retrievals, particularly SO_2 and HCHO. Using the OE method, the expected retrieval performance of GEMS has been assessed based on its design requirements, prelaunch calibration results, and synthetic radiances (Rodgers 2000; Jeong 2015; Zoogman et al. 2017). Detailed descriptions of the performance estimation and results can be found in the supplement, Fig. ES7, and Tables ES2 and ES3. Averaging kernels (AKs), which characterize the sensitivity of retrieved values to the true atmospheric quantities, are important tools in assessing the product accuracy. Diurnal variations of the ozone AK are shown in Fig. ES8 at selected hours on

Table ES4. Summary of validation network for GEMS products.

Network name	Network full name	Instrument	Observation	Reference (home page)	GEMS product
WOUDC	World Ozone and Ultraviolet Radiation Data Centre	Dobson spectrophotometer	TO3, O_3 umkehr	Fioletov et al. (1999) (https://woudc.org)	TO3, O_3 profile
		Brewer spectrophotometer	TO3, O_3 umkehr, AOD, SO_2 total column density, UV irradiance, UV index		TO3, SO_2, AOD, UV index
Pandora network	Pandora network	Pandora spectrometer	Total columns of O_3, NO_2, HCHO, their vertical profiles	Herman et al. (2009) (https://pandora.gsfc.nasa.gov, http://pandonia.net)	TO3, NO_2, HCHO
EANET	Acid Deposition Monitoring Network in East Asia	Wet and dry sampler	Wet deposition (sulfate), dry deposition (concentrations of SO_2, NO_2, and O_3)	Sugimoto and Uno (2009) (www.eanet.asia)	SO_2, NO_2, tropospheric O_3
MAX-DOAS network	Multi-Axis Differential Optical Absorption Spectroscopy network	MAX-DOAS	Tropospheric NO_2, AOD	Kanaya et al. (2014) (https://ebcrpa.jamstec.go.jp/maxdoashp)	Tropospheric NO_2, AOD
AD-NET	Asian dust and aerosol lidar observation network	Lidar	Extinction coefficients of attenuated backscatter, aerosol, dust, spherical particle	Sugimoto et al. (2016) (www-lidar.nies.go.jp/AD-Net)	AOD
KALION	Korea aerosol lidar observation network		Attenuated backscatter coefficient, aerosol extinction coefficient	Yeo et al. (2016) (www.kalion.kr)	
MPLNET	NASA Micro-Pulse lidar Network		Cloud heights, thin cloud extinction optical depths, cloud phase, aerosol height,[a] aerosol depolarization ratio profiles	Welton et al. (2001) (https://mplnet.gsfc.nasa.gov)	
AERONET	Aerosol Robotic Network	Sun photometer	Size distribution, refractive index, phase functions, water vapor, Angstrom exponent, fine mode fraction, AOD, SSA	Holben et al. (1998) (https://aeronet.gsfc.nasa.gov)	AOD, SSA
SONET	Sun–Sky Radiometer Observation Network	Sun photometer		Li et al. (2018) (https://aeronet.gsfc.nasa.gov)	
SKYNET	Sky radiometer network	Sky radiometer	AOD, SSA	Takamura and Nakajima (2004) (www.skynet-isdc.org)	
GAW WDCA	Global Atmosphere Watch World Data Centre for Aerosols	Aerosol sampler	Aerosol particle number concentration, size distribution, light scattering coefficient, AOD	WMO/GAW Rep. 153 (2003) (www.gaw-wdca.org)	AOD
Ceilometer network	Ceilometer network	Lidar	Cloud bottom height, cloud fraction	Münkel and Roininen (2010) (https://data.kma.go.kr/data/)	Cloud fraction

[a] Only available at AERONET observation times.

15 January. Diurnal variations of the AKs indicate enhanced retrieval sensitivity near the surface at noon and with decreasing sensitivity as SZA increases due to Rayleigh scattering and ozone absorption. Sensitivity near the surface peaks in July (not shown here) and decreases in other months as noontime SZA increases. Note that in this analysis, the VZA is fixed at 43° to represent the average viewing geometry of the GEO instrument. The degrees of freedom for signal (DFS) is a measure of the number of components of the profile retrieval not constrained by the a priori (Rodgers 2000). The GEMS performance estimation showed that the expected annual mean DFS for ozone is 0.8 ± 0.2 in the troposphere and 2.9 ± 0.5 in the stratospheric. The DFS increases by up to 20% with the binning of 8 spatial pixels.

Table ES5. Geostationary Air Quality Constellation (from CEOS).

	Sentinel-4	TEMPO	GEMS
Domain	Europe	North America	Asia–Pacific
Revisit	1 h	1 h	1 h
Planned launch	~2023	2022	2020
Payload	UV–Vis–NIR 305–500 nm 750–775 nm	UV–Vis 290–490 nm 540–740 nm	UV–Vis 300–500 nm
Products	O_3, trop. O_3, NO_2, SO_2, HCHO, AAI, AOD, height-resolved aerosol	O_3, trop. O_3, 0–2 km O_3, NO_2, HCHO, SO_2, CHOCHO, BrO, IO, HONO, AOD, AAI	O_3, NO_2, SO_2, HCHO, CHOCHO, AOD, AAI, AEH
Spatial sampling	8 km × 8 km at 45°N	≤2.2 km N/S × 5.2 km E/W at 36.5°N	3.5 km N/S × 8 km E/W at 38°N
Nominal product resolution	8.9 km N/S × 11.7 km E/W at 40°N	≤8.88 km N/S × 5.15 km E/W at 35°N	7 km N/S × 8 km E/W at 38°N (gas), 3.5 km N/S × 8 km E/W at 38°N (aerosol)
Accompanied instruments	MTG-S, MTG-I	GOES-R/S ABI	AMI, GOCI-2

Validation network

For the validation network within the GEMS FOR shown in Fig. 7, the details of each measurement network are listed in Table ES4, including instruments, measured parameters, and references.

Geostationary AQ constellation

In the framework of the Committee on Earth Observation Satellites' (CEOS) Atmospheric Composition Virtual Constellation (AC-VC) program, initiatives have been taken to enhance the relevance of the GEO AQ constellation missions (Table ES5) for related science and policy applications. To this end, AC-VC pursues harmonization of product quality, coordination of calibration and validation activities, and facilitates sharing and analysis of the mission on the global scale (CEOS 2011).

In the future, additional geostationary AQ missions will hopefully join this constellation, including the Geostationary Atmospheric Observation Satellite (Japan) and the Fengyun-4 (FY-4) mission (China), with hopes for South America, Africa, and the Middle East. These GEO AQ missions will be accompanied by meteorological instruments including the Advanced Baseline Imager (ABI), AMI, and the Flexible Combined Imager (FCI), which will significantly enhance our understanding of the globalization of tropospheric pollution and short-term climate change significantly.

Table ES6. Satellite instruments to observe air quality with operational periods.

Sensor	Years of operation	Reference
TOMS	October 1978–December 2006	Heath et al. (1975)
GOES-8 imager	April 1994–May 2004	Menzel and Purdom (1994)
GOME	April 1995–July 2011	Burrows et al. (1993)
SeaWiFS	August 1997–December 2010	McClain et al. (2004)
MISR	December 1999–present	Diner et al. (1998)
MODIS	December 1999–present	Levy et al. (2013)
MOPITT	December 1999–present	Deeter et al. (2003)
SCIAMACHY	March 2002–April 2012	Bovensmann et al. (1999)
AIRS	May 2002–present	Aumann et al. (2003)
SEVIRI	August 2002–present	Aminou et al. (1997)
OMI	July 2004–present	Levelt et al. (2018)
TES	July 2004–present	Beer et al. (2001)
MTSAT imager	February 2006–May 2016	Miyamura (2007)
GOME-2	October 2006–present	Munro et al. (2016)
IASI	October 2006–present	Clerbaux et al. (2009)
GOCI	June 2010–present	Choi et al. (2012), Choi et al. (2016)
MI	June 2010–present	Kim et al. (2016)
CrIS	October 2011–present	Han et al. (2013)
OMPS	October 2011–present	Flynn et al. (2014)
VIIRS	October 2011–present	Jackson et al. (2013)
INSAT-3D imager	July 2013–present	Singh et al. (2016)
AHI	October 2014–present	Bessho et al. (2016), Lim et al. (2018)
EPIC	February 2015–present	Marshak et al. (2018)
ABI	November 2016–present	Schmit et al. (2017)
AGRI	December 2016–present	Yang et al. (2017)
TROPOMI	October 2017–present	Veefkind et al. (2012)
SGLI	December 2017–present	Imaoka et al. (2010)
EMI	May 2018–present	Zhang et al. (2018)
AMI	December 2018–present	Choi and Ho (2015), Park et al. (2016)
GEMS	Launch in 2020	This paper
GOCI-2	Launch in 2020	Ahn et al. (2010)
TEMPO	Launch in 2022	Zoogman et al. (2017)
FCI	Launch in 2021	Ouaknine et al. (2017)
3MI	Launch in 2022	Fougnie et al. (2018)
Sentinel-4	Launch in 2023	Ingmann et al. (2012)
MAIA	TBD	Diner et al. (2018)

TEMPO

The TEMPO (http://tempo.si.edu) satellite instrument will measure atmospheric pollution over North America, ranging from Mexico City to the Canadian oil sands, and from the Atlantic to the Pacific. Its high temporal resolution (hourly or better in daylight, with selected observations at 10 min or better) and high spatial resolution (10 km^2 at the center of the FOR) can resolve pollution sources at the sub-urban scale, improves emission inventories, monitors population exposure, and enables effective emission-control strategies. TEMPO will measure

O_3 profiles down to the boundary layer, along with NO_2, SO_2, H_2CO, $C_2H_2O_2$, H_2O, BrO, IO, HONO, clouds, and aerosols. Applications for these measurements include intercontinental pollution transport, biomass burning and O_3 production, aerosol products in concert with synergistic GOES IR measurements, lightning NO_x, soil NO_x and fertilizer application, crop and forest damage from O_3, chlorophyll and primary productivity, foliage studies, halogens in coastal and lake regions, ship tracks and drilling platform plumes, water vapor studies including atmospheric rivers, hurricanes, and corn sweat, volcanic emissions, high-resolution pollution versus traffic patterns; tidal effects on estuarine circulation and outflow plumes; and AQ response to power blackouts and other exceptional events. The instrument has been delivered and is awaiting spacecraft integration and launch in the next several years. Further details can be found in Zoogman et al. (2017).

Sentinel-4 UVN. The Sentinel-4 (S4) mission is part of the Copernicus Space Component. It has been designed to serve the needs of the Copernicus Atmosphere Monitoring Service for atmospheric composition observations over Europe with a fast revisit time (hourly) at a high spatial resolution (8 km N/S × 8 km E/W at 45°N). The key level-2 products of the Sentinel-4 mission cover total and tropospheric columns of O_3 and NO_2, total columns of SO_2, HCHO, CHOCHO, and aerosol parameters (optical depth, layer height, and UV absorbing index). Auxiliary products cover cloud properties (optical depth, fraction, and height) and surface reflectance characteristics. The S4 mission represents the European component of the geostationary Earth orbit (GEO) AQ constellation.

The S4 mission is implemented as a series of two imaging spectrometers with bands in the UV, Vis, and NIR (UVN) spectral domain, deployed on the Meteosat Third Generation Sounder (MTG-S) platforms. ESA is responsible for the mission implementation. Two S4/UVN instruments will be flown in sequence spanning an expected mission lifetime of 15 years. EUMETSAT will operate the S4/UVN instruments and will process mission data up to level 2. Further details can be found in Ingmann et al. (2012).

Relevant satellite instruments to observe air quality shown in Fig. 1 are listed in Table ES6 with operation period and references.

REFERENCES

Ahn, Y.-H., J.-H. Ryu, S. Cho, and S.-H. Kim, 2010: Missions and user requirements of the 2nd Geostationary Ocean Color Imager (GOCI-II). *Korean J. Remote Sens.*, **26**, 277–285.

Aminou, D. M. A., B. Jacquet, and F. Pasternak, 1997: Characteristics of the Meteosat Second Generation (MSG) radiometer/imager: SEVIRI. *Proc. SPIE*, **3221**, 19–31, https://doi.org/10.1117/12.298084.

Aumann, H. H., and Coauthors, 2003: AIRS/AMSU/HSB on the Aqua mission: Design, science objectives, data products, and processing systems. *IEEE Trans. Geosci. Remote Sens.*, **41**, 253–264, https://doi.org/10.1109/TGRS.2002.808356.

Beer, R., T. A. Glavich, and D. M. Rider, 2001: Tropospheric emission spectrometer for the Earth Observing System's Aura satellite. *Appl. Opt.*, **40**, 2356–2367, https://doi.org/10.1364/AO.40.002356.

Bessho, K., and Coauthors, 2016: An introduction to Himawari-8/9—Japan's new-generation geostationary meteorological satellites. *J. Meteor. Soc. Japan*, **94**, 151–183, https://doi.org/10.2151/jmsj.2016-009.

Bovensmann, H., J. P. Burrows, M. Buchwitz, J. Frerick, S. Noël, V. V. Rozanov, K. V. Chance, and A. P. H. Goede, 1999: SCIAMACHY: Mission Objectives and Measurement Modes. *J. Atmos. Sci.*, **56**, 127–150, https://doi.org/10.1175/1520-0469(1999)056<0127:SMOAMM>2.0.CO;2.

Burrows, J. P., and Coauthors, 1993: Global Ozone Monitoring Experiment (GOME): Interim science report. ESA Rep. SP-1151, 60 pp.

CEOS, 2011: A geostationary satellite constellation for observing global air quality: An International Path Forward. CEOS Atmospheric Composition Constellation Rep., 41 pp.

Choi, J.-K., Y. J. Park, J. H. Ahn, H.-S. Lim, J. Eom, and J.-H. Ryu, 2012: GOCI, the world's first geostationary ocean color observation satellite, for the monitoring of temporal variability in coastal water turbidity. *J. Geophys. Res.*, **117**, C09004, https://doi.org/10.1029/2012JC008046.

Choi, M., and Coauthors, 2016: GOCI Yonsei Aerosol Retrieval (YAER) algorithm and validation during the DRAGON-NE Asia 2012 campaign. *Atmos. Meas. Tech.*, **9**, 1377–1398, https://doi.org/10.5194/amt-9-1377-2016.

Choi, W. J., and Coauthors, 2018: Introducing the Geostationary Environment Monitoring Spectrometer. *J. Appl. Remote Sens.*, **13**, 044005, https://doi.org/10.1117/1.JRS.12.044005.

Choi, Y. S., and C. H. Ho, 2015: Earth and environmental remote sensing community in South Korea: A review. *Remote Sens. Appl. Soc. Environ.*, **2**, 66–76, https://doi.org/10.1016/J.RSASE.2015.11.003.

Clerbaux, C., and Coauthors, 2009: Monitoring of atmospheric composition using the thermal infrared IASI/MetOp sounder. *Atmos. Chem. Phys.*, **9**, 6041–6054, https://doi.org/10.5194/acp-9-6041-2009.

Deeter, M. N., and Coauthors, 2003: Operational carbon monoxide retrieval algorithm and selected results for the MOPITT instrument. *J. Geophys. Res.*, **108**, 4399, https://doi.org/10.1029/2002JD003186.

Diner, D. J., and Coauthors, 1998: Multi-angle Imaging Spectroradiometer (MISR) instrument description and experiment overview. *IEEE Trans. Geosci. Remote Sens.*, **36**, 1072–1087, https://doi.org/10.1109/36.700992.

——, and Coauthors, 2018: Advances in multiangle satellite remote sensing of speciated airborne particulate matter and association with adverse health effects: From MISR to MAIA. *J. Appl. Remote Sens.*, **12**, 042603, https://doi.org/10.1117/1.JRS.12.042603.

Fioletov, V. E., J. B. Kerr, E. W. Hare, G. J. Labow, and R. D. McPeters, 1999: An assessment of the world ground-based total ozone network performance from the comparison with satellite data. *J. Geophys. Res.*, **104**, 1737–1747, https://doi.org/10.1029/1998JD100046.

Flynn, L., and Coauthors, 2014: Performance of the Ozone Mapping and Profiler Suite (OMPS) products. *J. Geophys. Res. Atmos.*, **119**, 6181–6195, https://doi.org/10.1002/2013JD020467.

Fougnie, B., and Coauthors, 2018: The Multi-Viewing Multi-Channel Multi-Polarisation Imager—Overview of the 3MI polarimetric mission for aerosol and cloud characterization. *J. Quant. Spectrosc. Radiat. Transfer*, **219**, 23–32, https://doi.org/10.1016/j.jqsrt.2018.07.008.

Han, Y., and Coauthors, 2013: Suomi NPP CrIS measurements, sensor data record algorithm, calibration and validation activities, and record data quality. *J. Geophys. Res. Atmos.*, **118**, 12 734–12 734, https://doi.org/10.1002/2013JD020344.

Heath, D. F., A. J. Krueger, H. A. Roeder, and B. D. Henderson, 1975: The Solar Backscatter Ultraviolet and Total Ozone Mapping Spectrometer (SBUV/TOMS) for NIMBUS G. *Opt. Eng.*, **14**, 323–331, https://doi.org/10.1117/12.7971839.

Herman, J., N. Abuhassan, A. Cede, G. Mount, E. Spinei, and M. Tzortziou, 2009: NO_2 column amounts from ground-based Pandora and MFDOAS spectrometers using the direct-sun DOAS technique: Intercomparisons and application to OMI validation. *J. Geophys. Res.*, **114**, D13307, https://doi.org/10.1029/2009JD011848.

Holben, B. N., and Coauthors, 1998: AERONET—A federated instrument network and data archive for aerosol characterization. *Remote Sens. Environ.*, **66**, 1–16, https://doi.org/10.1016/S0034-4257(98)00031-5.

Imaoka, K., and Coauthors, 2010: Global Change Observation Mission (GCOM) for monitoring carbon, water cycles, and climate change. *Proc. IEEE*, **98**, 717–734, https://doi.org/10.1109/JPROC.2009.2036869.

Ingmann, P., B. Veihelmann, J. Langen, D. Lamarre, H. Stark, and G. B. Courrèges-Lacoste, 2012: Requirements for the GMES Atmosphere Service and ESA's implementation concept: Sentinels-4/-5 and -5p. *Remote Sens. Environ.*, **120**, 58–69, https://doi.org/10.1016/j.rse.2012.01.023.

Jackson, J. M., H. Liu, I. Laszlo, S. Kondragunta, L. A. Remer, J. Huang, and H. C. Huang, 2013: Suomi-NPP VIIRS aerosol algorithms and data products. *J. Geophys. Res. Atmos.*, **118**, 12 673–12 689, https://doi.org/10.1002/2013JD020449.

Jeong, U., 2015: Error analysis and characterization of the atmospheric trace gas and aerosol inversion products from the hyper-spectral remote sensing measurements based on the optimal estimation method. Ph.D. thesis, Yonsei University, 147 pp.

Kanaya, Y., and Coauthors, 2014: Long-term MAX-DOAS network observations of NO_2 in Russia and Asia (MADRAS) during the period 2007-2012: Instrumentation, elucidation of climatology, and comparisons with OMI satellite observations and global model simulations. *Atmos. Chem. Phys.*, **14**, 7909–7927, https://doi.org/10.5194/acp-14-7909-2014.

Kim, M., and Coauthors, 2016: Aerosol optical properties derived from the DRAGON-NE Asia campaign, and implications for a single-channel algorithm to retrieve aerosol optical depth in spring from Meteorological Imager (MI) onboard the Communication, Ocean, and Meteorological Satellit (COMS). *Atmos. Chem. Phys.*, **16**, 1789–1808, https://doi.org/10.5194/acp-16-1789-2016.

Kleipool, Q. L., M. R. Dobber, J. F. de Haan, and P. F. Levelt, 2008: Earth surface reflectance climatology from 3 years of OMI data. *J. Geophys. Res.*, **113**, D18308, https://doi.org/10.1029/2008JD010290.

Levelt, P. F., and Coauthors, 2018: The Ozone Monitoring Instrument: Overview of 14 years in space. *Atmos. Chem. Phys.*, **18**, 5699–5745, https://doi.org/10.5194/acp-18-5699-2018.

Levy, R. C., S. Mattoo, L. A. Munchak, L. A. Remer, A. M. Sayer, F. Patadia, and N. C. Hsu, 2013: The Collection 6 MODIS aerosol products over land and ocean. *Atmos. Meas. Tech.*, **6**, 2989–3034, https://doi.org/10.5194/amt-6-2989-2013.

Li, Z. Q., and Coauthors, 2018: Comprehensive study of optical, physical, chemical, and radiative properties of total columnar atmospheric aerosols over China: An overview of Sun–Sky Radiometer Observation Network (SONET) measurements. *Bull. Amer. Meteor. Soc.*, **99**, 739–755, https://doi.org/10.1175/BAMS-D-17-0133.1.

Lim, H., M. Choi, J. Kim, Y. Kasai, and P. W. Chan, 2018: AHI/Himawari-8 Yonsei aerosol retrieval (YAER): Algorithm, validation and merged products. *Remote Sens.*, **10**, 699, https://doi.org/10.3390/RS10050699.

Marshak, A., and Coauthors, 2018: Earth observations from *DSCOVR* EPIC instrument. *Bull. Amer. Meteor. Soc.*, **99**, 1829–1850, https://doi.org/10.1175/BAMS-D-17-0223.1.

McClain, C. R., G. C. Feldman, and S. B. Hooker, 2004: An overview of the SeaWiFS project and strategies for producing a climate research quality global ocean

bio-optical time series. *Deep-Sea Res. II*, **51**, 5–42, https://doi.org/10.1016/j.dsr2.2003.11.001.

Menzel, W. P., and J. F. W. Purdom, 1994: Introducing GOES-I: The first of a new generation of geostationary operational environmental satellites. *Bull. Amer. Meteor. Soc.*, **75**, 757–781, https://doi.org/10.1175/1520-0477(1994)075<0757:IGITFO>2.0.CO;2.

Miyamura, K., 2007: MTSAT-2 systems (in Japanese). JMA Meteorological Satellite Center Tech. Note, Vol. 49, 4 pp.

Molod, A., L. Takacs, M. Suarez, and J. Bacmeister, 2015: Development of the GEOS-5 atmospheric general circulation model: Evolution from MERRA to MERRA2. *Geosci. Model Dev.*, **8**, 1339–1356, https://doi.org/10.5194/gmd-8-1339-2015.

Münkel, C., and R. Roininen, 2010: Automatic monitoring of boundary layer structures with ceilometers. *Vaisala News*, No. 184, Vaisala, Helsinki, Finland, 7–9.

Munro, R., and Coauthors, 2016: The GOME-2 instrument on the MetOp series of satellites: Instrument design, calibration, and level 1 data processing—An overview. *Atmos. Meas. Tech.*, **9**, 1279–1301, https://doi.org/10.5194/amt-9-1279-2016.

Ouaknine, J., and Coauthors, 2017: The FCI on board MTG: Optical design and performances. *Proc. SPIE*, **10563**, 1056323, https://doi.org/10.1117/12.2304144.

Park, J.-H., J.-Y. Bok, H.-O. H.-S. Lim, and D.-W. Chung, 2016: Development of radiometric calibration system for GEO-KOMPSAT-2 AMI. *SpaceOps 2016 Conf.*, Daejeon, Korea, American Institute of Aeronautics and Astronautics, 2325, https://doi.org/10.2514/6.2016-2325.

Rodgers, C. D., 2000: *Inverse Methods for Atmospheric Sounding: Theory and Practice.* World Scientific, 256 pp.

Schmit, T. J., P. Griffith, M. M. Gunshor, J. M. Daniels, S. J. Goodman, and W. J. Lebair, 2017: A closer look at the ABI on the GOES-R series. *Bull. Amer. Meteor. Soc.*, **98**, 681–698, https://doi.org/10.1175/BAMS-D-15-00230.1.

Singh, R., S. P. Ojha, C. M. Kishtawal, P. K. Pal, and A. S. Kiran Kumar, 2016: Impact of the assimilation of INSAT-3D radiances on short-range weather forecasts. *Quart. J. Roy. Meteor. Soc.*, **142**, 120–131, https://doi.org/10.1002/qj.2636.

Sugimoto, N., and I. Uno, 2009: Observation of Asian dust and air-pollution aerosols using a network of ground-based lidars (ADNet): Real time data processing for validation/assimilation of chemical transport models. *IOP Conf. Ser. Earth Environ. Sci.*, **7**, 012003, https://doi.org/10.1088/1755-1307/7/1/012003.

——, T. Nishizawa, A. Shimizu, and Y. Jin, 2016: The Asian Dust and Aerosol Lidar Observation Network (AD-Net). *27th Int. Laser Radar Conf.*, New York, NY, NOAA, 19001, https://doi.org/10.1051/epjconf/201611919001.

Takamura, T., and T. Nakajima, 2004: Overview of SKYNET and its activities. *Opt. Puray Apl.*, **37**, 3303–3308.

Veefkind, J. P., and Coauthors, 2012: TROPOMI on the ESA Sentinel-5 Precursor: A GMES mission for global observations of the atmospheric composition for climate, air quality and ozone layer applications. *Remote Sens. Environ.*, **120**, 70–83, https://doi.org/10.1016/j.rse.2011.09.027.

Welton, E. J., J. R. Campbell, J. D. Spinhirne, and V. S. Scott III, 2001: Global monitoring of clouds and aerosols using a network of micropulse lidar systems. *Proc. SPIE*, **4153**, 151–158, https://doi.org/10.1117/12.417040.

Yang, J., Z. Zhang, C. Wei, F. Lu, and Q. Guo, 2017: Introducing the new generation of Chinese geostationary weather satellites, Fengyun-4. *Bull. Amer. Meteor. Soc.*, **98**, 1637–1658, https://doi.org/10.1175/BAMS-D-16-0065.1.

Yeo, H., and Coauthors, 2016: The KALION automated aerosol type classification and mass concentration calculation algorithm. *Korean J. Remote Sens.*, **32**, 119–131, https://doi.org/10.7780/kjrs.2016.32.2.5.

Zhang, C., and Coauthors, 2018: Preflight evaluation of the performance of the Chinese Environmental Trace Gas Monitoring Instrument (EMI) by spectral analyses of nitrogen dioxide. *IEEE Trans. Geosci. Remote Sens.*, **56**, 3323–3332, https://doi.org/10.1109/TGRS.2018.2798038.

Zoogman, P., and Coauthors, 2017: Tropospheric Emissions: Monitoring of Pollution (TEMPO). *J. Quant. Spectrosc. Radiat. Transfer*, **186**, 17–39, https://doi.org/10.1016/j.jqsrt.2016.05.008.